A STUDY ON STRUCTURAL INTEGRITY OF DISSIMILAR WELDS IN NUCLEAR PIPING

Jong-Sung Kim
Korea Power Engineering Company, Yongin, Kyunggi-do, Republic of Korea
Phone: 82-31-289-4278,
Fax: 82-31-289-3189
E-mail: kimjs@kopec.co.kr

Tae-Eun Jin
Korea Power Engineering Company, Yongin, Kyunggi-do, Republic of Korea
Phone: 82-31-289-4282,
Fax: 82-31-289-3189
E-mail: jinte@kopec.co.kr

Seung-Gun Lee
Korea Power Engineering Company, Yongin, Kyunggi-do, Republic of Korea
Phone: 82-31-289-4278
E-mail: gun@kopec.co.kr

Han-Sub Chung
Korea Electric Power Research Institute, Daejeon, Republic of Korea
Phone: 82-42-865-5530
E-mail: hschung@kepri.re.kr

ABSTRACT

Dissimilar welds in nuclear piping such as a reactor pressure vessel outlet nozzle-safe end weld have been known to experience some primary water stress corrosion cracking due to synchronism of three principal factors, tensile welding residual stresses, susceptible materials and corrosive environment. In order to evaluate structural integrity of the nuclear piping with dissimilar welds during design or lifetime extension stages, it is necessary to assess the effects of geometric variables, strength mismatch, tensile residual stresses, etc. on stress corrosion crack initiation and growth of the dissimilar welds reliably and efficiently. The purpose of this study is to develop the robust formulae of crack driving parameters such as stress intensity factor and J-integral as well as residual stress distributions in the dissimilar welds by using finite element analysis. First, tensile properties on dissimilar welds are locally measured by tensile tests. Second, the formulae for residual stress distributions are developed based on the parametric study results via the finite element analysis adequately considering the effect of geometric variables and mismatch on real dissimilar welds. Last, the formulae for crack driving parameters are developed by the parametric study results parametric study results via the finite element analysis in order to investigate the effects of strength mismatch and secondary stress.

Keywords: dissimilar welds, nuclear piping, tensile properties, residual stresses, stress intensity factor, J-integral, tensile test, finite element analysis, structural integrity.

1. INTRODUCTION

Dissimilar welds in nuclear piping such as a reactor pressure vessel outlet nozzle-safe end weld have been known to experience some primary water stress corrosion cracking due to synchronism of three principal factors, tensile welding residual stresses, susceptible materials and corrosive environment. In order to evaluate structural integrity of the nuclear piping with dissimilar welds during design or lifetime extension stages, it is necessary to assess the effects of geometric variables, strength mismatch, tensile residual stresses, etc. on stress corrosion crack initiation and growth of the dissimilar welds reliably and efficiently. By the way, it is difficult to find the study developing the formulae of crack driving parameters such as stress intensity factor and J-integral as well as residual stress distributions in the dissimilar welds.

Therefore, the purpose of this study is to develop the robust formulae of residual stress distributions and crack driving parameters in the dissimilar welds by using finite element analysis. First, tensile properties on dissimilar welds are locally measured by tensile tests[1]. Second, the formulae for residual stress distributions are developed based on the parametric study results via the finite element analysis adequately considering the effect of geometric variables and mismatch on real dissimilar welds[2]. Last, the formulae for crack driving parameters are developed by the parametric study results via the finite element analysis in order to investigate the effects of strength mismatch and secondary stress such as residual stress[3].

2. MEASUREMENT OF TENSILE PROPERTIES

2.1 Materials and Welding

Base materials used to construct dissimilar welds are SA508 Gr.3 low alloy steel and F316 stainless steel. Both base metals are provided as forged and heat treated condition and prepared as 40mm thick plate before the welding. The plates are welded manually, closely simulating the welding procedures used for the real nozzle to pipe welding. The schematics of welding procedure are shown in Figure 2. After the buttering of 2 passes on the machined edge of SA508 Gr.3 plate, the pieces were post weld heat treated at 615^{o}C to relieve residual stresses. The first 2-3 passes of V-groove welding were completed by GTAW with alloy 82 bare wires, then the remaining thickness was filled by SMAW with alloy 182 electrode.

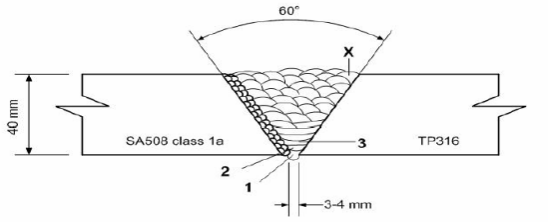

Fig. 1 Schematics of the dissimilar weld of single V-groove design

2.2 Tensile Tests and Variation of Tensile Properties

Small size round bar tensile specimens and mini-sized sheet type tensile specimens shown in figure 2 were machined from the welded plates. As shown in Figure 3, the specimens were taken from SA508 low alloy steel region, alloy 82/182 weld region, and stainless steel region along the welding direction. In addition, 6 small size specimens were taken along the transverse direction. The specimens were tested at room temperature at strain rate of $5x10^{-4}$/sec.

Figure 4 shows the round bar tensile test results. The test results show a little different property depending on the test position, across the dissimilar weld and along the thickness of weld. As a whole, SA508 base metals showed higher yield strength and ultimate strength than alloy 82/182 weld and TP316. On the average, the yield strengths of SA508 are about 450MPa, but those of alloy 82/182 are about 350MPa, far lower than base metals. However, the ultimate strengths of alloy 82/182 welds are similar as those of SA508 and SS316 base metals.

Figure 5 shows the mini tensile test results. First of all, it is shown in the figure that the overall values of tensile properties measured using mini specimens are compatible with those measured using round bar specimens. However, unlike the round bar test results, the differences in tensile properties, especially the ultimate strength between SA508, alloy 82/182 and SS316 are more clearly shown in mini tensile specimen test results. Also, it is found that the differences are greater at the top part of the weld and become smaller at the bottom part near weld root pass.

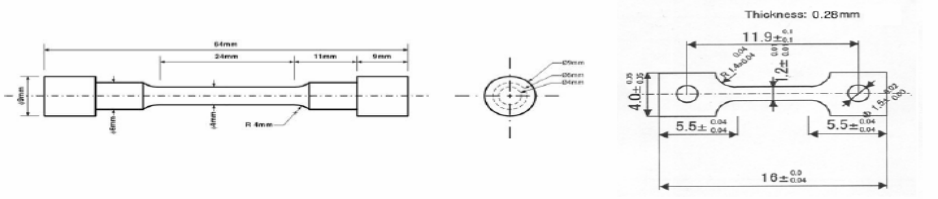

(a) small size specimen (b) mini size specimen

Fig. 2 Tensile test specimens

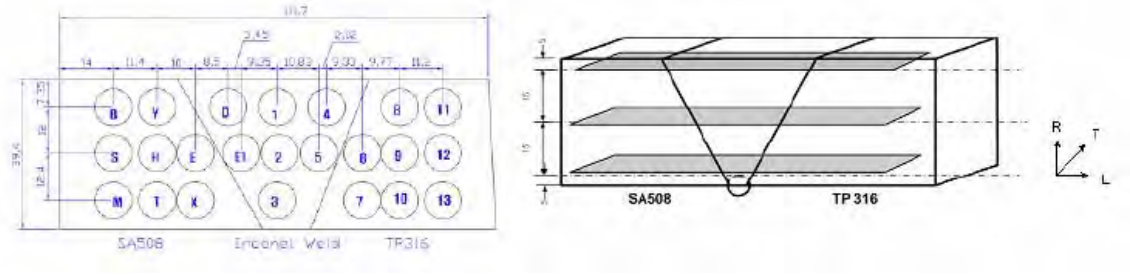

(a) small size specimen (b) mini size specimen

Fig. 3 Location of the tensile specimens taken from the dissimilar weld

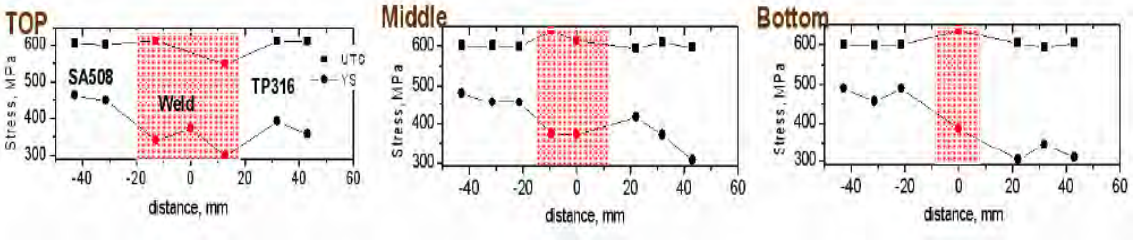

Fig. 4 Variation of tensile properties across the dissimilar weld using small size specimens

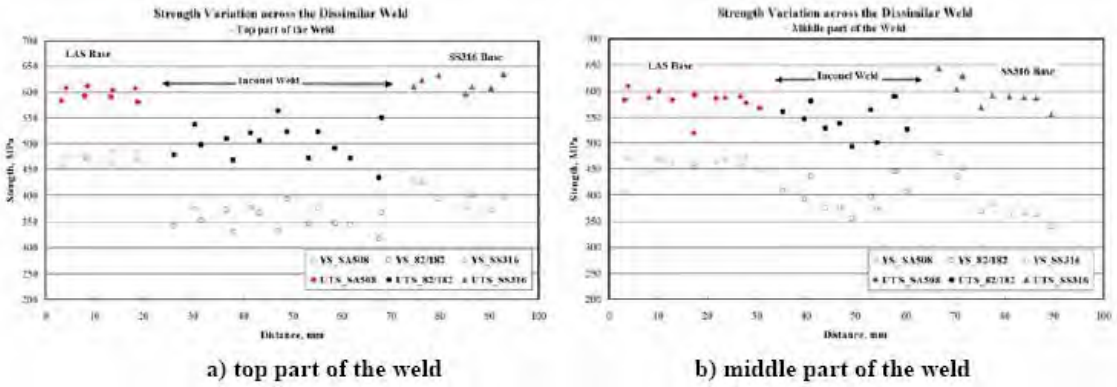

a) top part of the weld b) middle part of the weld

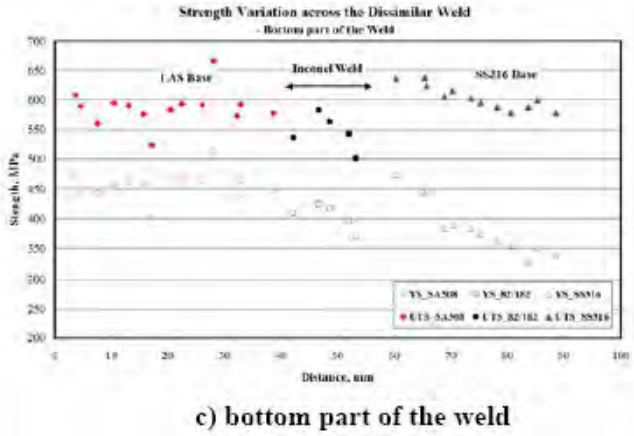

c) bottom part of the weld

Fig. 5 Variation of tensile properties across the dissimilar weld using mini size speciemens

3. FORMULATION OF RESIDUAL STRESS DISTRIBUTION

3.1 Residual Stress Analysis

The finite element for a pressurizer spray nozzle, which is made of of SA508 Gr.3, SA541 Gr.3, SA182 F316, and alloy 82/182, and has one dissimilar weld, is shown in Figure 6. The number of element and node is 1530 and 1687, respectively. The 8-node axis-symmetric element is used for temperature and residual stress analyses.

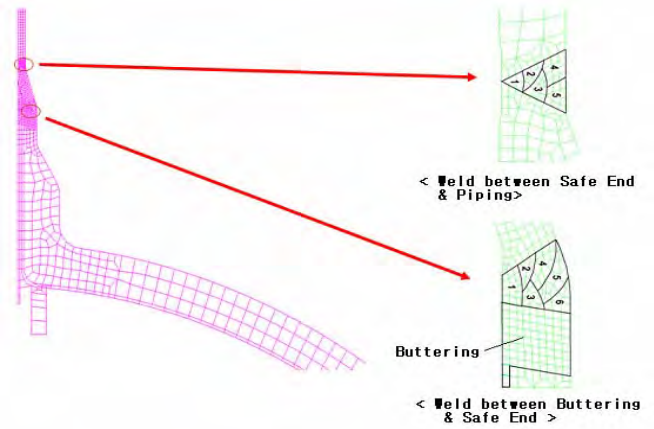

Fig. 6 Finite element model for parametric study

Figure 7 shows the variation of residual stress distributions, which is normalized by yielding strength of alloy 82/182 weldment at room temperature, on welding center line according to thickness increase under constant thickness ratio (R_i/t=4). The axial residual stress distributions on welding center line in the figure are changed from global bending type[4] to local bending type[4] according to thickness increase. The hoop residual stresses near the inner and outer surfaces are respectively more compressive and tensile with thickness increase. Figure 8 illustrates the variation of normalized residual stress distributions according to thickness ratio increase under fixed thickness (t=25.27mm). As shown in Figure 8, the axial residual stresses on inner and outer surface increase according to thickness ratio increase. Also, it can be found that the axial residual stresses for the most inner region decrease according to thickness ratio increase. The hoop residual stresses near the inner surface significantly increase according to thickness ratio increase. Figure 9 shows the variation of normalized residual stress distributions on welding center line according to yielding strength increase. As depicted in the figure, the normalized residual stresses on welding center line have insignificantly different distributions according to yielding strength. And, it is found that the residual stresses aren't linearly proportional to yielding strength of weldment.

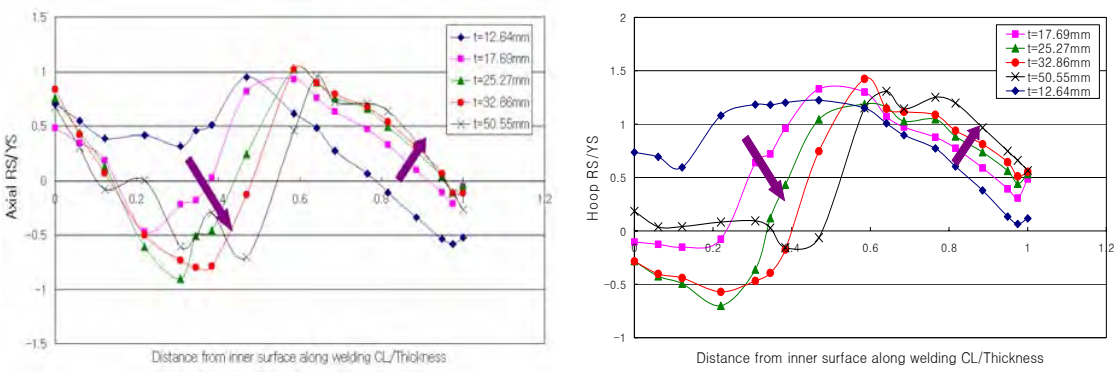

(a) axial residual stress (b) hoop residual stress

Fig. 7 Variation of residual stress distributions with thickness increase

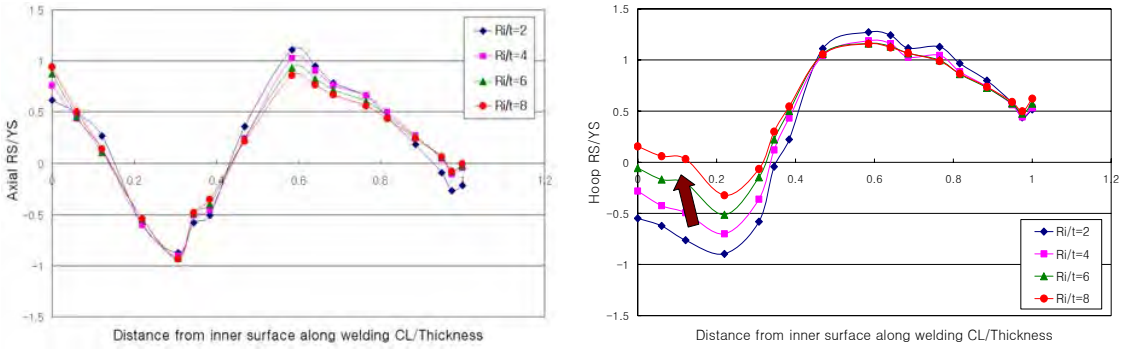

(a) axial residual stress (b) hoop residual stress

Fig. 8 Variation of residual stress distributions with thickness ratio increase

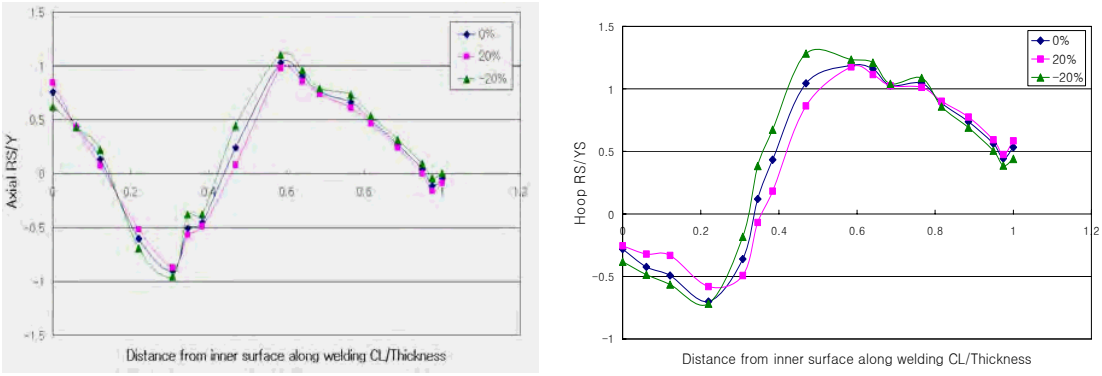

(a) axial residual stress (b) hoop residual stress

Fig. 9 Variation of axial residual stress distributions with yield strength increase

3.2 Formulation and Verification

Based on parametric study results, the following equations are derived for axial residual stress distributions by decomposing membrane, bending and self-equilibrium component:

$$\sigma^r(\frac{x}{t}) = \sigma_m^r + \sigma_b^r\{1-2(\frac{x}{t})\} + \sum_{i=0}^{6} A_i(\frac{x}{t})^i \,, \tag{1}$$

$$\sigma_m^r = \{-0.0003(\frac{R_i}{t})^2 - 0.0017(\frac{R_i}{t}) + 0.1981\}F_m(\frac{t}{t_0})F_{YSm}(\frac{\sigma_{ys}}{\sigma_{ys0}}) \qquad (1.5 \le \frac{R_i}{t} \le 10)\,, \tag{2}$$

$$\sigma_b^r = \{-0.002(\frac{R_i}{t})^3 + 0.0372(\frac{R_i}{t})^2 - 0.2008(\frac{R_i}{t}) + 0.0064\}F_b(\frac{t}{t_0})F_{YSb} \qquad (1.5 \le \frac{R_i}{t} \le 10)\,, \tag{3}$$

$$A_0 = \{0.0017(\frac{R_i}{t})^3 - 0.0367(\frac{R_i}{t})^2 + 0.2857(\frac{R_i}{t}) + 0.1936\}F_{A0}(\frac{t}{t_0})\,, \tag{4}$$

$$A_1 = \{-0.0385(\frac{R_i}{t})^3 + 0.9458(\frac{R_i}{t})^2 - 7.9052(\frac{R_i}{t}) + 23.2601\}F_{A1}(\frac{t}{t_0})\,, \tag{5}$$

$$A_2 = \{0.3488(\frac{R_i}{t})^3 - 8.3658(\frac{R_i}{t})^2 + 67.915(\frac{R_i}{t}) - 315.18\}F_{A2}(\frac{t}{t_0})\,, \tag{6}$$

$$A_3 = \{-1.4222(\frac{R_i}{t})^3 + 32.255(\frac{R_i}{t})^2 - 248.081(\frac{R_i}{t}) + 1260.8\}F_{A3}(\frac{t}{t_0})\,, \tag{7}$$

$$A_4 = \{2.7218(\frac{R_i}{t})^3 - 58.914(\frac{R_i}{t})^2 + 430.48(\frac{R_i}{t}) - 2166.1\}F_{A4}(\frac{t}{t_0}), \quad (8)$$

$$A_5 = \{-2.4114(\frac{R_i}{t})^3 + 50.398(\frac{R_i}{t})^2 - 352.55(\frac{R_i}{t}) + 1696.3\}F_{A5}(\frac{t}{t_0}), \quad (9)$$

$$A_6 = \{0.8006(\frac{R_i}{t})^3 - 16.297(\frac{R_i}{t})^2 + 109.98(\frac{R_i}{t}) - 500.1\}F_{A6}(\frac{t}{t_0}), \quad (10)$$

where σ_m^r is transverse membrane residual stress component for the fixed condition at pipe end, σ_b^r is transverse bending stress component, σ_{ys} is yielding strength, σ_{ys0} is reference yielding strength(=393.6931MPa), t_0 is reference thickness(=25.27mm), F_m, F_b and F_{Ai} are specific functions of t/t_0, F_{YSm} and F_{YSb} are specific functions of σ_{ys}/σ_{ys0}, x is through thickness distance from inner surface .

Finally, the formulae are verified by comparing with the previous results such as PVRC JIP[5] and API 579[6]. Figure 10 represents the comparison with the previous results. As depicted in the figure, it is identified that the engineering formulae can be a valid and available tool evaluating the axial residual stress distributions along welding centerline on the dissimilar welds of nozzle in nuclear piping.

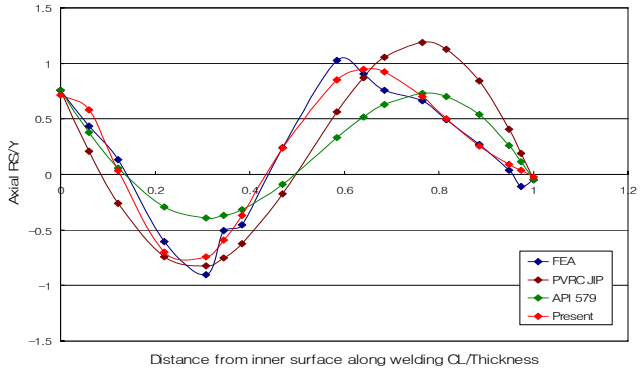

Fig. 10 Comparison with the previous results(R_i/t=4, t=25.27mm)

4. FORMULATION OF FRACTURE MECHANICS PARAMETERS

4.1 Effect of Yield Strength Mismatch on J-Integral

Figure 11 shows the finite element EPFM (elasto-plastic fracture mechanics) analysis results for the dissimilar pipe with circumferential through wall crack located on weld center under primary loading. As shown in Figure 11, the effect of yield strength mismatch on J-integral is within 5% for the over-mismatch case. The following J-integral and COD equations are derived considering the mismatch effect from the figures:

$$\frac{J}{J_e} = \frac{COD}{COD_e} = \frac{E\varepsilon_{ref}}{L_r\sigma_{YS}} + \frac{1}{2}L_r^3\frac{\sigma_{YS}}{E\varepsilon_{ref}} \quad (11)$$

$$L_r = M / M_{OR} \quad (12)$$

$$M_{OR} = \gamma(\theta/\pi)M_L \quad (13)$$

$$\gamma(\theta/\pi) = 0.82 + 0.75(\theta/\pi) + 0.42(\theta/\pi)^2 \quad (14)$$

4.2 Effect of Secondary Stress on J-Integral

Figure 12 and 13 show the finite element EPFM analysis results for the dissimilar pipe with circumferential through wall crack located on weld center under primary and secondary loading. L_r is the ratio of primary stress to limit load. Ψ is the ratio of secondary stress to limit load. V is the variable to quantify the effect of secondary stress on elasto-plastic fracture. V_o is the value of V under only secondary loading. As shown in Figure 12 and 13, the effect of secondary stress on J-integral increases with decrease of primary stress. And, it is found that V/V_o is

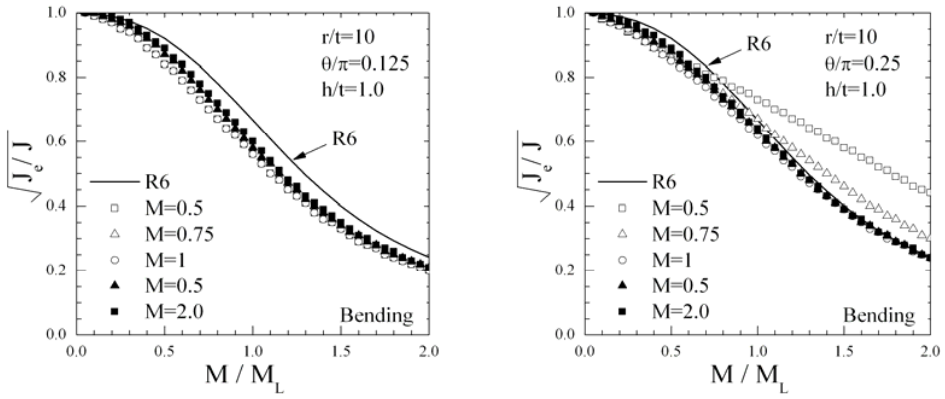

(a) θ/π=0.125 (b) θ/π=0.25

Fig. 11 J-integral values for the dissimilar pipe with through wall crack located on weld center

maximized at Lr=0.8 and approaches near zero if L_r is greater than 1.5. The following J –integral and COD equations are derived considering the effect of secondary stress:

$$\frac{J^{p+s}}{J_e^p}=\frac{COD^{p+s}}{COD_e^p}=(1+V\frac{K^s}{K^p})^2(\frac{E\varepsilon_{ref}}{L_r\sigma_{YS}}+\frac{1}{2}L_r^3\frac{\sigma_{YS}}{E\varepsilon_{ref}}) \tag{15}$$

$$\frac{V}{V_0}=1+0.2L_r+(1+2L_r)(0.02\frac{K_p^s}{K^p/L_r}) \quad \text{(lower } L_r\text{)}$$

$$\frac{V}{V_0}=3.1-2L_r \quad (L_r<1.35) \tag{16}$$

$$\frac{V}{V_0}=0.4 \quad (L_r>1.35)$$

$$V_0=\sqrt{\frac{J^s}{J_e^s}} \tag{17}$$

$$\Psi=\frac{K^s}{K^p/L_r} \tag{18}$$

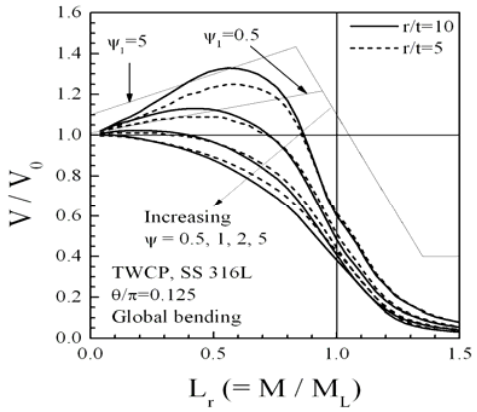

Fig. 12 Variations of V/V_0 vs. L_r for the dissimilar pipe with center crack pipe (global bending)

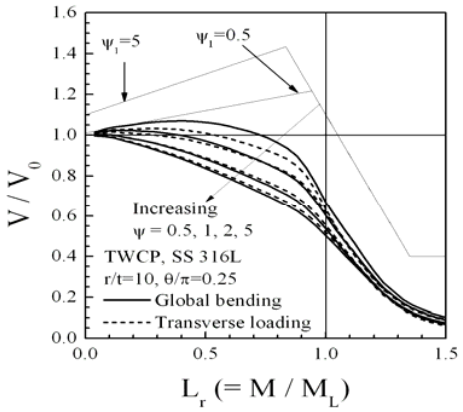

Fig. 13 Variations of V/V_0 vs. L_r for the dissimilar with center crack (global bending/transverse loading)

5. CONCLUSIONS

A study on structural integrity of dissimilar welds in nuclear piping was performed by using tensile test and finite element analysis. From this study, some major findings are obtained as follows:

- SA508 base metals have higher yield strength and ultimate strength than alloy 82/182 weld and TP316 while the ultimate strengths of alloy 82/182 welds are similar as those of SA508 and SS316 base metals.
- Engineering formulae of residual stress distributions are developed based on parametric study results and they can be a valid and available tool evaluating the axial residual stress distributions along welding centerline on the dissimilar welds of nozzle in nuclear piping.
- J-integral and COD equations are derived considering the effect of mismatch and secondary stress based on the parametric study results.

REFERENCES

1. J.H. Lee, C.H. Jang, J.S. Kim, and T.E. Jin, "Spatial variation of mechanical properties in alloy 82/182 dissimilar metal welds," Proceedings of ASINCO 6, 2006.
2. J.S. Kim and T.E. Jin, "Development of engineering formula for welding residual stress distributions of dissimilar welds on nozzle in nuclear component," Proceedings of ASME PVP 2007, 2007.
3. C.K. Oho, T.K. Song, Y.J. Kim, J.S. Kim, and T.E. Jin, Development of Design and Lifetime Evaluation Technologies for Dissimilar Welds on Nuclear Piping, the 2nd Year Report, 2007.
4. Battelle, Critical Assessment, Validation, and Recommendations on Residual Stress Estimates for Fitness for Service Assessment, PVRC Residual Stress and Local PWHT JIP, Task 0 Report, 2001.
5. Battelle, Investigation of Welding Residual Stresses and Local Post-Weld Heat Treatment, Final PVRC Residual Stress and Local PWHT JIP, Final Report, 2002.
6. P. Dong and Z. Cao, "Mechanics basis of residual stress profiles for new API 579 Appendix E," Proceedings of ASME PVP 2006, 2006.

